Chapter 8
Noise Sensitivity Evaluation of Autoregressive Features Extracted from Structure Vibration

Ruigen Yao and Shamim N. Pakzad

Abstract In the past few decades many types of structural damage indices based on structural health monitoring signals have been proposed, requiring performance evaluation and comparison studies on these indices in a quantitative manner. One tool to help accomplish this objective is analytical sensitivity analysis, which has been successfully used to evaluate the influences of system operational parameters on observable characteristics in many fields of study. In this chapter, the sensitivity expressions of two damage features, namely the Mahalanobis distance of autoregressive coefficients and Cosh distance of autoregressive spectra, will be derived with respect to the measurement noise level. The effectiveness of the proposed methods is illustrated in a numerical case study on a 10 DOF system, where their results are compared with those from direct simulation and theoretical calculation.

Keywords Sensitivity analysis • Structural vibration monitoring • Autoregressive modeling • Autoregressive spectrum estimation • Yule-Walker method

8.1 Introduction

Damage detection is a very crucial part in the regular assessment and maintenance routine for civil infrastructure. Traditionally this task is carried out by human inspection, and thereby is expensive, time consuming, and the accuracy relies on individual expertise. Recently, the advancements in sensing and computational technology have made it feasible for a sensor network to be installed on a civil structure, and data collected from the sensors will then be processed to produce information pertaining to the structural condition. To date many research studies in the literature [1–4] devoted to this topic can be found, forming a promising branch of study often referred to as data-driven structural health monitoring (SHM). Ideally, the new system will cost less than traditional method because of the lowering prices of sensing systems, and produce more accurate and reliable decisions that are free of human judgment bias or expertise. Moreover, SHM has the capability to reveal problems undetectable via 'naked-eye' inspection such as internal fracture and delamination.

Vibration responses (e.g. acceleration, strain) are among the most commonly measured signals for structural monitoring purposes. One category of widely employed vibration-based damage indices consists of modal properties extracted using system identification/modal realization approaches [5–7]. Recently, many alternative damage features [8–10] based on structural output are proposed to address the computational efficiency (especially for time domain extraction algorithms) issues concerning modal properties estimators [1]. Time series analysis [11] for single channel acceleration measurements is one of the notable techniques attempted in a number of research articles [12–15], where algorithms such as scalar autoregressive (AR), autoregressive/autoregressive with exogenous input (AR-ARX), autoregressive with moving average (ARMA) modeling have been applied and functions of estimated model parameters used as damage features. These features are reported to be less complicated to compute and more sensitive to local damage in their respective applications.

While it is important to propose and test new features to improve the state-of-the -art of structural damage detection, examination of the effect of environmental and operational factors on established features in an analytically rigorous manner is also crucial for optimal feature selection for different practices. Previously, research has been conducted on evaluating the

R. Yao (✉) • S.N. Pakzad
Department of Civil and Environmental Engineering, Lehigh University, Bethlehem, PA18015, USA
e-mail: ruy209@Lehigh.edu; pakzad@Lehigh.edu

H.S. Atamturktur et al. (eds.), *Model Validation and Uncertainty Quantification, Volume 3: Proceedings of the 32nd IMAC, A Conference and Exposition on Structural Dynamics, 2014*, Conference Proceedings of the Society for Experimental Mechanics Series, DOI 10.1007/978-3-319-04552-8_8,

adverse effect of measurement noise on the accuracy of estimated modal parameters [16]. In this chapter, the sensitivity of two damage features based on AR modeling due to measurement noise is studied and an analysis methodology is proposed. The two methods are the Mahalanobis distance [17] of AR coefficients and the Cosh distance [18] of AR model spectra between the baseline state and the current state. The validity of this methodology is supported by simulation results from a 10 DOF bridge model.

The paper is organized as follows: Sect. 8.2 contains stepwise derivations regarding the analysis for the sensitivity with respect to measurement noise for both features. In Sect. 8.3, sensitivity analysis is applied to a 10-DOF simulated model and the results are compared with those from direct simulation and theoretical calculation. Conclusions are then made on the efficiency of the algorithms and the effectiveness of the features.

8.2 Measurement Noise Sensitivity for the AR Damage Features

Distance measures between characteristics of undamaged and damaged structure state are often adopted as damage features. Damage features examined in this chapter are the Mahalanobis distance of AR coefficients and the Cosh distance of AR model spectra extracted from structural acceleration measurements [14]. The definition of a univariate AR model of order p is [19]:

$$x(t) = \sum_{j=1}^{p} \varphi_j x(t-j) + \epsilon_x(t). \tag{8.1}$$

In this equation, $x(t)$ is the time series to be analyzed, φ_j terms are the AR model coefficients, and $\epsilon_x(t)$ is the model residual. Mahalanobis distance, which in this case operates on AR coefficient vectors, is a metric to evaluate the deviation within vectorial Gaussian sample groups [17]. Its definition is stated as below:

$$D^2(\boldsymbol{\varphi}_u, \overline{\boldsymbol{\varphi}}_b) = \left(\boldsymbol{\varphi}_u^T - \overline{\boldsymbol{\varphi}}_b^T\right) \boldsymbol{\Sigma}_b^{-1} \left(\boldsymbol{\varphi}_u - \overline{\boldsymbol{\varphi}}_b\right). \tag{8.2}$$

where φ_u is the feature vector from the unknown structural state and $\overline{\boldsymbol{\varphi}}_b / \boldsymbol{\Sigma}_b$ is the mean/covariance of feature vectors from baseline state. When the unknown vector φ_u is not generated from the baseline distribution, it is expected that the distance value will increase significantly.

From each vector of AR coefficients, corresponding AR spectrum plot can be constructed:

$$S_{AR}^{(p)}(\omega) = \frac{\sigma_e^2}{\left|\boldsymbol{\varphi}\left(e^{j\omega}\right)\right|^2} = \frac{\sigma_e^2}{\left|\sum_{k=0}^{p} \varphi_k e^{-j\omega k}\right|^2}, \tag{8.3}$$

where $\varphi_0 = 1$. For feature extraction purposes model residual variance σ_e^2 is not calculated and set to unity, since its value is determined by excitation level. Cosh spectral distance based on AR spectrum estimates can be used as a frequency domain alternative to Mahalanobis distance of AR coefficients:

$$C\left(\mathbf{S}, \overline{\mathbf{S}}_b\right) = \frac{1}{2N} \sum_{j=1}^{N} \left[\frac{S\left(\omega_j\right)}{\overline{S}_b\left(\omega_j\right)} + \frac{\overline{S}_b\left(\omega_j\right)}{S\left(\omega_j\right)} - 2 \right]. \tag{8.4}$$

where $\overline{\mathbf{S}}_b$ is the baseline spectrum, $\mathbf{S}$ is the spectrum from the unknown state, and N is the length of each spectrum vector. An illustration of the procedures through which the features are generated is also given in Fig. 8.1. To get the noise sensitivity of both indices, the analysis is divided into four steps according to the feature extraction procedures.

8.2.1 Theoretical Expression of Structural Response Autocovariance Function (ACF)

An AR model is an all-pole system. In [15] it is stated that the ith mode of N degrees-of-freedom system corresponds to a conjugate pair of discrete system poles:

$$z_i, z_i^* = e^{-\zeta_i \omega_{ni} T_s \pm j\sqrt{1-\zeta_i^2}\omega_{ni} T_s}. \tag{8.5}$$

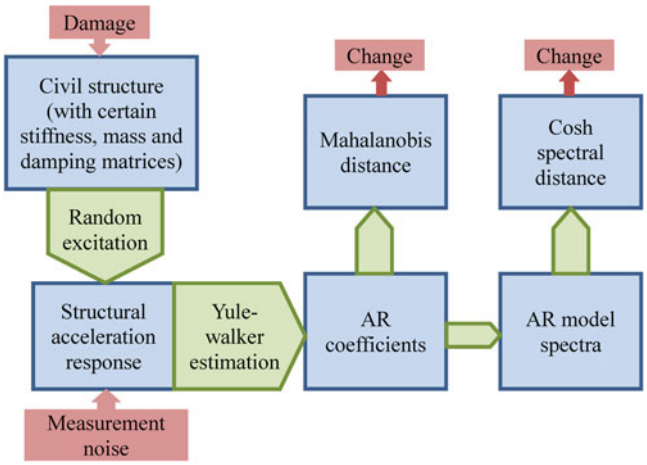

Fig. 8.1 Illustration of the relation between structural damage/measurement noise and AR-based damage features

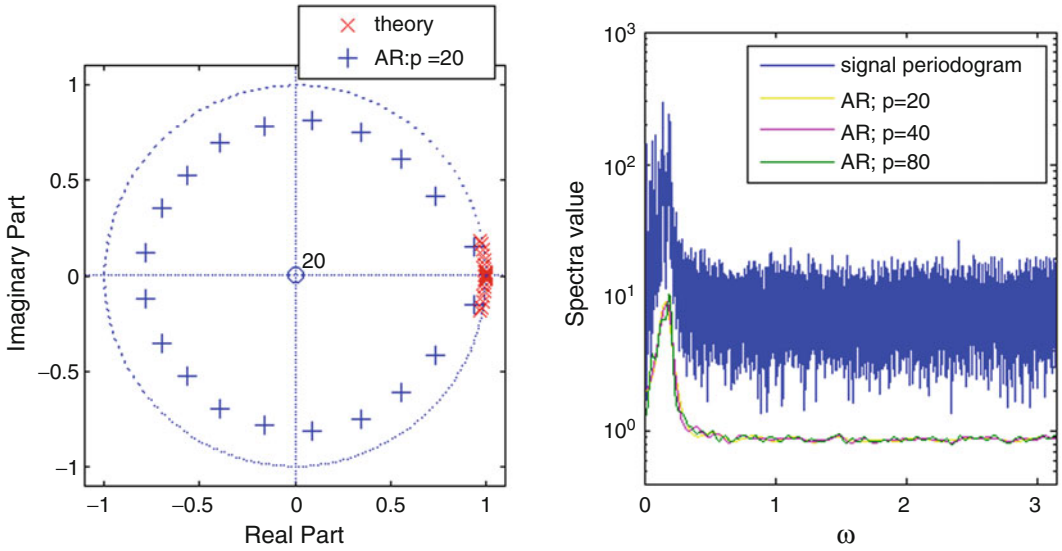

Fig. 8.2 The contrast of the theoretical pole positions from digital signal processing theory and those from estimated AR models (*left plot*) and the comparison of the signal periodogram and the AR model spectra of different orders (*right plot*)

where $\omega_{\mathrm{n}i}$ and ζ_i are the modal frequency and damping ratio of the ith mode, respectively. T_{s} is the sampling frequency of the measurement signals. If it is assumed that the estimated AR model exactly captures all system poles, then an AR coefficient vector of size $(2N \times 1)$ can be computed by utilizing relations between polynomial coefficients and roots. However, simulation analysis reveals that there is a very large difference between the theoretical poles and those estimated from AR modeling (Fig. 8.2). Also noted from Fig. 8.2 is that AR spectrum does not converge to resemble the envelope of signal periodogram as the model order increases. Therefore, the theoretical expression of system ACF, from which the AR coefficient estimators are computed, is investigated here as a first step towards obtaining accurate sensitivity estimates for both features.

To start, take the Laplace transform of the displacement impulse response of the ith system mode [20]:

$$h_i(t) = \frac{1}{m_i \omega_{\mathrm{D}i}} \mathrm{e}^{-\zeta_i \omega_{\mathrm{n}i} t} \sin \omega_{\mathrm{D}i} t. \quad \overset{L.T.}{\Rightarrow} \quad \widehat{h}_i(s) = \frac{1}{m_i \left(s^2 + 2\zeta_i \omega_{\mathrm{n}i} s + \omega_{\mathrm{n}i}^2\right)} \tag{8.6}$$

Here m_i and $\omega_{\mathrm{D}i}$ are the modal mass and damped frequency of the ith mode. From the relationship between modal and nodal input/response in structural dynamics the impulse response matrix and the Laplace transfer function of the whole system can be obtained as:

$$\mathbf{H}(t) = \mathbf{\Phi} diag\left(h_i(t)\right) \mathbf{\Phi}^{\mathrm{T}}, \quad \widehat{\mathbf{H}}(s) = \mathbf{\Phi} diag\left(\widehat{h}_i(s)\right) \mathbf{\Phi}^{\mathrm{T}} = \left(\mathbf{M}s^2 + \mathbf{C}s + \mathbf{K}\right)^{-1},$$

$$\mathbf{u}(t) = \mathbf{H} \otimes \mathbf{p}(t), \;\; \widehat{\mathbf{u}}(s) = \widehat{\mathbf{H}}(s)\widehat{\mathbf{p}}(s). \tag{8.7}$$

where $\mathbf{M}$, $\mathbf{C}$ and $\mathbf{K}$ are the mass, damping and stiffness matrices of the system, and $\otimes$ stands for the convolution operation. When the external excitation is a random process, the covariance of the response $\mathbf{u}$ can be represented as [21]:

$$\mathbf{R}_u(\tau) = E\left(\mathbf{u}(t)\mathbf{u}(t+\tau)^T\right) = E\left([\mathbf{H} \otimes \mathbf{p}](t)\,[\mathbf{H} \otimes \mathbf{p}](t+\tau)^T\right) = \left[\mathbf{H} \oplus \mathbf{R}_p \otimes \mathbf{H}\right](\tau). \tag{8.8}$$

Here $\oplus$ represents the cross-correlation between two signals and $\mathbf{R}_p(\tau)$ is the covariance matrix of input excitation. From the convolution theorem, the Fourier Transform of the response covariance matrix, also known as the response power spectral density, is related to the excitation power spectral density through (8.9):

$$\therefore \widehat{\mathbf{R}}_u(i\omega) = \widehat{\mathbf{H}}^*(i\omega)\,\widehat{\mathbf{R}}_p(i\omega)\,\widehat{\mathbf{H}}(i\omega) = \mathbf{\Phi} diag\left(\widehat{h}_i(i\omega)\right)^* \mathbf{\Phi}^T \widehat{\mathbf{R}}_p(i\omega)\,\mathbf{\Phi} diag\left(\widehat{h}_i(i\omega)\right)\mathbf{\Phi}^T. \tag{8.9}$$

In the case of white noise excitation, the ACF between displacement responses at node i and node j is obtained by taking the inverse Laplace Transform of (8.9), (same result can be achieved through performing time domain convolution/correlation in (8.8))

$$\begin{aligned}
\mathbf{R}_u(\tau)_{\{i,j\}} &= \sum_{r=1}^{N} \frac{\phi_i^r}{m_r \omega_{\mathrm{D}r}} \sum_{s=1}^{N}\sum_{k=1}^{N}\sum_{l=1}^{N} \beta_{jkl}^{rs} \left(J_{rs}^2 + I_{rs}^2\right)^{-\frac{1}{2}} \exp\left(-\zeta_r \omega_{\mathrm{n}r}\tau\right) \sin\left(\omega_{\mathrm{D}r}\tau + \gamma_{rs}\right), \\
\beta_{jkl}^{rs} &= \frac{\mathbf{R}_p(0)_{\{k,l\}}\phi_k^r \phi_j^s \phi_l^s}{m_s}, \;\; I_{rs} = 2\omega_{\mathrm{D}r}\left(\zeta_r \omega_{\mathrm{n}r} + \zeta_s \omega_{\mathrm{n}s}\right), \\
J_{rs} &= \left({\omega_{\mathrm{D}s}}^2 - {\omega_{\mathrm{D}r}}^2\right) + \left(\zeta_r \omega_{\mathrm{n}r} + \zeta_s \omega_{\mathrm{n}s}\right)^2, \;\; \tan\gamma_{rs} = \frac{I_{rs}}{J_{rs}}.
\end{aligned} \tag{8.10}$$

where $(\cdot)_{\{k,l\}}$ refers to the term in kth row and lth column of the subscripted matrix and ϕ_i^r is the ith component of mode shape r. This formulation is very similar to that given by [22]; only that an additional dimension of summation is introduced to account for possible spatial correlation among inputs at system DOFs. The ACF of acceleration measurements can be obtained by taking the fourth derivative of (8.10) and adding an impulse term to the expression,

$$\begin{aligned}
\mathbf{R}_{\ddot{u}}(\tau)_{\{i,j\}} &= E\left(H^{'}(0)p(t)p(t)^T H^{'}(0)\right)_{\{i,j\}} + \frac{\mathrm{d}^4\left[\mathbf{R}_u(\tau)_{\{i,j\}}\right]}{\mathrm{d}\tau^4} \\
&= \Phi\Phi^T R_p \Phi\Phi^T{}_{\{i,j\}} + \sum_{r=1}^{N} \frac{\phi_i^r}{m_r \omega_d^r} \sum_{s=1}^{N}\sum_{k=1}^{N}\sum_{l=1}^{N} \beta_{jkl}^{rs} \left(J_{rs}^2 + I_{rs}^2\right)^{-\frac{1}{2}} \omega_{\mathrm{n}r}^4 \exp\left(-\zeta_r \omega_{\mathrm{n}}^r \tau\right) \\
&\quad \left\{\left[\left(1-7\zeta_r^2\right)\left(1-\zeta_r^2\right) + \zeta_r^4\right]\sin\left(\omega_{\mathrm{D}r}\tau + \gamma_{rs}\right) + 4\zeta_r\left(1-2\zeta_r^2\right)\left(1-\zeta_r^2\right)^{\frac{1}{2}}\cos\left(\omega_{\mathrm{D}r}\tau + \gamma_{rs}\right)\right\}.
\end{aligned} \tag{8.11}$$

This expression will be used to compute the baseline and theoretical value of features in the next section.

8.2.2 *Sensitivity of the AR Coefficients/Spectra to the Increase in the Noise Level*

To compute the influence of noise on damage feature estimation, consider the signal covariance sequence of contaminated signals. When white noise of standard deviation σ is added to the signal, its ACF sequence R_c will be

$$R_c(\tau) = R(\tau) + R_n(\tau) = R(\tau) + \sigma^2\delta(\tau), \tag{8.12}$$

where $R_n(\tau)$ denotes the ACF of white noise. Therefore, the sensitivity of the estimated coefficients using Yule-Walker method [11] to the variance of additive Gaussian noise will be

$$\frac{\mathrm{d}\left[\widehat{\varphi}_1, \widehat{\varphi}_2, \ldots, \widehat{\varphi}_p\right]^T}{\mathrm{d}\sigma^2} = \frac{\mathrm{d}\left[\left(\boldsymbol{\Gamma} + \sigma^2\mathbf{I}\right)^{-1}\boldsymbol{\gamma}\right]}{\mathrm{d}\sigma^2} = -\boldsymbol{\Gamma}^{-2}\boldsymbol{\gamma}. \tag{8.13}$$

Where Γ is the Toeplitz matrix consisting of signal ACF values from lag 0 to p-1, and Y is a vector containing signal ACF values from lag 1 to p. For the AR spectrum, the definition here states that it is:

$$\widehat{S}_{AR}^{(p)}(\omega) = \frac{1}{\left|\widehat{\varphi}\left(e^{j\omega}\right)\right|^2} = \frac{1}{\left|\sum_{k=0}^{p}\widehat{\varphi}_k e^{-j\omega k}\right|^2}, \tag{8.14}$$

In this definition, $\widehat{\varphi}_0 = 1$. Its sensitivity to changes in coefficients can be computed as:

$$\frac{d\widehat{S}_{AR}^{(p)}(\omega)^{-1}}{d\widehat{\varphi}_k} = 2Re\left\{e^{-j\omega k}\left(\sum_{n=0}^{p}\widehat{\varphi}_n e^{j\omega n}\right)\right\}, \quad \frac{d\widehat{S}_{AR}^{(p)}(\omega)}{d\widehat{\varphi}_k} = -2Re\left\{e^{-j\omega k}\left(\sum_{n=0}^{p}\widehat{\varphi}_n e^{j\omega n}\right)\right\}\widehat{S}_{AR}^{(p)}(\omega)^2. \tag{8.15}$$

Thus by combining (8.13) and (8.15) the sensitivity of the spectrum to ACF changes is calculated.

It should be noted that (8.13) only accounts for the extreme case (i.e. number of samples $N_s = \infty$). For the finite sample scenario, the ACF of both the original and the contaminated signal is also affected by estimation errors and exhibits an asymptotic Gaussian distribution [11]. To avoid unnecessary statistical complexities and focus on the direct influence of measurement noise level on damage features here it is assumed that the ACF estimators are exact (the asymptotic case).

8.2.3 *Sensitivity of the Distance Measures to Changes in AR Coefficients/Spectra*

The theoretical feature values under the null hypothesis will be needed for evaluation of relative sensitivity. The AR coefficient estimators are asymptotically unbiased and follow a multivariate Gaussian distribution with covariance matrix $\frac{\sigma_e^2}{N}\boldsymbol{\Gamma}^{-1}$ ($\sigma_e^2 = R(0) - \boldsymbol{\gamma}^T\boldsymbol{\Gamma}^{-1}\boldsymbol{\gamma}$) [11]. Under this assumption, the Mahalanobis distance feature for the undamaged structural state has a chi-square distribution with p degrees-of-freedom, and its statistical expectation is p. The expression for the expected value of the Mahalanobis distance for the general case is presented in (8.16).

$$\begin{aligned} E\left(D^2\right) &= E\left(\boldsymbol{\varphi}_u^T - \overline{\boldsymbol{\varphi}}_b^T\right)\boldsymbol{\Sigma}_b^{-1}\left(\boldsymbol{\varphi}_u - \overline{\boldsymbol{\varphi}}_b\right) = E\left[\left(\boldsymbol{\varphi}_u^T - \overline{\boldsymbol{\varphi}}_u^T\right)\boldsymbol{\Sigma}_b^{-1}\left(\boldsymbol{\varphi}_u - \overline{\boldsymbol{\varphi}}_u\right)\right] + \left[\left(\overline{\boldsymbol{\varphi}}_u^T - \overline{\boldsymbol{\varphi}}_b^T\right)\boldsymbol{\Sigma}_b^{-1}\left(\overline{\boldsymbol{\varphi}}_u - \overline{\boldsymbol{\varphi}}_b\right)\right] \\ &= trace\left[\boldsymbol{\Sigma}_b^{-1}\boldsymbol{\Sigma}_u\right] + \left[\left(\overline{\boldsymbol{\varphi}}_u^T - \overline{\boldsymbol{\varphi}}_b^T\right)\boldsymbol{\Sigma}_b^{-1}\left(\overline{\boldsymbol{\varphi}}_u - \overline{\boldsymbol{\varphi}}_b\right)\right], \end{aligned} \tag{8.16}$$

The first and second order sensitivities of $E(D^2)$ to signal covariance can then be computed. Note that for notation simplicity, θ is used to express the ACF value at an arbitrary lag.

$$\left.\frac{dE\left(D^2\right)}{d\theta}\right|_{\boldsymbol{\varphi}_u=\boldsymbol{\varphi}_b,\boldsymbol{\Sigma}_u=\boldsymbol{\Sigma}_b} = trace\left[\boldsymbol{\Sigma}_b^{-1}\frac{d\boldsymbol{\Sigma}_u}{d\theta}\right], \tag{8.17}$$

$$\left.\frac{d^2E\left(D^2\right)}{d\theta^2}\right|_{\boldsymbol{\varphi}_u=\boldsymbol{\varphi}_b,\boldsymbol{\Sigma}_u=\boldsymbol{\Sigma}_b} = trace\left[\boldsymbol{\Sigma}_b^{-1}\frac{d^2\boldsymbol{\Sigma}_u}{d\theta^2}\right] + 2\left[\frac{d\left(\overline{\boldsymbol{\varphi}}_u^T - \overline{\boldsymbol{\varphi}}_b^T\right)}{d\theta}\boldsymbol{\Sigma}_b^{-1}\frac{d\left(\overline{\boldsymbol{\varphi}}_u - \overline{\boldsymbol{\varphi}}_b\right)}{d\theta}\right]. \tag{8.18}$$

The contribution of the first and second order sensitivity of $\boldsymbol{\Sigma}_u$ with respect to the feature value is relatively small compared to the mean shift in the application described in the following section. Under the Gaussian assumption, the AR spectral estimates also asymptotically follow a normal distribution; as p^3/N decreases, $\sqrt{\frac{N}{p}}\left(\overline{S}_b - S\right)/\overline{S}_b$ converges to a

normal distribution with asymptotic variance equals to four at DC and two otherwise [23]. Therefore the expected value for the Cosh distance of the baseline state can be written as the sum of moments of this Gaussian distribution:

$$E(C)\Big|_{ES(\omega_j)=\overline{S}_b(\omega_j)} = \frac{1}{2N}\sum_{j=1}^{N} E\left[\frac{S(\omega_j)}{\overline{S}_b(\omega_j)} + \frac{\overline{S}_b(\omega_j)}{S(\omega_j)} - 2\right]$$
$$= \frac{1}{2N}\sum_{j=1}^{N} E\left[\frac{\overline{S}_b(\omega_j)}{S(\omega_j)} - 1\right] = \frac{1}{2N}\sum_{j=1}^{N} E\left[\frac{1}{(S(\omega_j)-\overline{S}_b(\omega_j))/\overline{S}_b(\omega_j)+1} - 1\right],$$

The following is obtained after performing a geometric series expansion on $\left(S\left(\omega_j\right) - \overline{S}_b\left(\omega_j\right)\right)/\overline{S}_b\left(\omega_j\right)$ for the equation above:

$$E(C)\Big|_{ES(\omega_j)=\overline{S}_b(\omega_j)} = \frac{1}{2N}\sum_{j=1}^{N} E\left[\sum_{l=1}^{\infty}\left(\frac{\mathrm{S}\left(\omega_\mathrm{j}\right) - \overline{S}_b\left(\omega_j\right)}{\overline{S}_b\left(\omega_j\right)}\right)^{2l}\right]. \tag{8.19}$$

Since the normal assumption is valid only in the asymptotic sense, and higher order statistical moments are less significant in value and affected more by the deviation from this assumption, only the first two terms ($l = 1, 2$) will be considered in applications in this chapter. The sensitivity expressions of Cosh distance are obtained in a similar manner as that for Mahalanobis distance,

$$\frac{dE(C)}{d\theta}\Big|_{ES(\omega_j)=\overline{S}_\mathrm{b}(\omega_\mathrm{j})} = \frac{1}{2N}\sum\nolimits_1^{\mathrm{N}}\left\{\frac{\mathrm{d}ES\left(\omega_\mathrm{j}\right)}{\mathrm{d}\theta}\frac{1}{\overline{S}_\mathrm{b}\left(\omega_\mathrm{j}\right)} + \frac{\mathrm{d}E\left[S\left(\omega_\mathrm{j}\right)^{-1}\right]}{\mathrm{d}\theta}\overline{S}_\mathrm{b}\left(\omega_\mathrm{j}\right)\right\}$$
$$= \frac{1}{2N}\sum\nolimits_1^{\mathrm{N}}\left\{\frac{\mathrm{d}ES\left(\omega_\mathrm{j}\right)}{\mathrm{d}\theta}\frac{1}{\overline{S}_\mathrm{b}\left(\omega_\mathrm{j}\right)} + \frac{\mathrm{d}\sum_{l=0}^{\infty}E\left(\frac{\overline{S}_b(\omega_j)-S(\omega_\mathrm{j})}{\overline{S}_b(\omega_j)}\right)^{l}}{\mathrm{d}\theta}\right\} = 0, \tag{8.20}$$

$$\frac{d^2E(C)}{d\theta^2}\Big|_{S(\omega_j)=\overline{S}_\mathrm{b}(\omega_\mathrm{j})} = \frac{1}{2N}\sum\nolimits_1^{\mathrm{N}}\left\{\frac{\mathrm{d}^2ES\left(\omega_\mathrm{j}\right)}{\mathrm{d}\theta^2}\frac{1}{\overline{S}_\mathrm{b}\left(\omega_\mathrm{j}\right)} + \frac{\mathrm{d}^2\sum_{l=0}^{\infty}E\left(\frac{\overline{S}_b(\omega_j)-S(\omega_\mathrm{j})}{\overline{S}_b(\omega_j)}\right)^{l}}{\mathrm{d}\theta^2}\right\}$$
$$= \frac{1}{2N}\sum\nolimits_1^{\mathrm{N}}\left(\frac{\mathrm{d}S\left(\omega_\mathrm{j}\right)}{\mathrm{d}\theta}\right)^2\frac{2}{\overline{S}_\mathrm{b}\left(\omega_\mathrm{j}\right)^2}. \tag{8.21}$$

The noise sensitivities of both features are found as the product of the sensitivities of features to ACF and the sensitivities of ACF to structural measurement noise.

8.3 Simulation Example: Sensitivity Analysis for a 10-DOF Structure

To verify the sensitivity analysis scheme presented in the previous section, it is applied to a 10-DOF model with linear topology and simply supported at both ends (Fig. 8.3). The mass of each node is 2 tons, the length of each element is 25 m and the section stiffness (EI) is $2.5 \times 10^5\ kN \cdot m^2$.

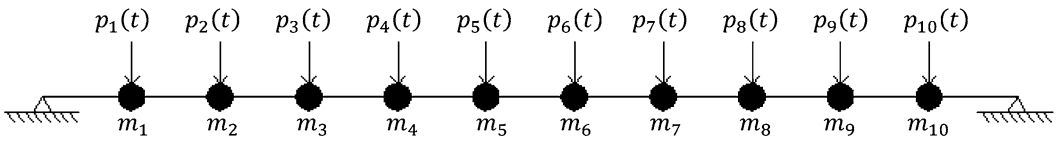

Fig. 8.3 The simulated 10 DOF model

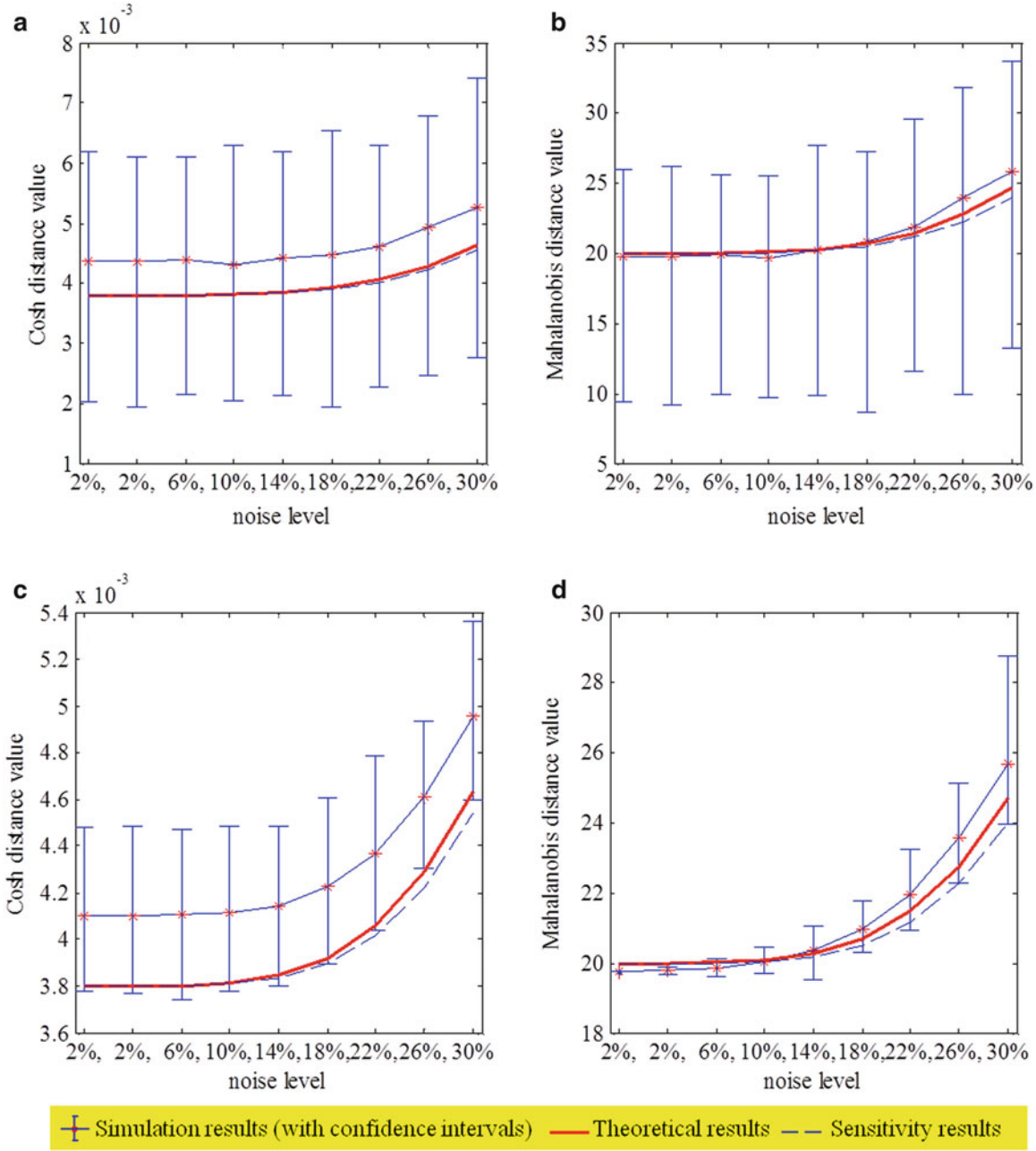

Fig. 8.4 Plots of the Mahalanobis distance and Cosh distance damage feature values as noise level increases. Plots (**a**, **b**): simulation results from one experiment; (**c**, **d**): the average simulation results from 50 runs (confidence intervals are constructed based on average values)

Spatially and chronologically uncorrelated random excitation is applied at each node of the system. Acceleration signals are simulated from the system using Newmark's method, and both feature values are extracted from the signals during multiple runs of simulation. These simulation results regarding effects of measurement noise on feature values are compared with theoretical analysis results and sensitivity analysis results. Here theoretical results refer to that computed directly from the theoretical ACF for each measurement noise case. For all simulations and computations, the AR model order is set at 20. During each run of simulation, 88 signal segments, each containing 5,400 data points sampled at a frequency of 50 Hz, are used to calculate the Mahalanobis distance and Cosh distance features.

Figure 8.4 shows the trends of Mahalanobis distance and Cosh distance as the noise level increases. All data are collected at node 4. Signals with 2 % noise level are used as baseline and another case with 2 % noise level is included for false positive testing. It can be seen that the 3 lines have relatively close values in comparison to the 95 % confidence interval from one simulation, thereby demonstrating the validity and effectiveness of the tangent sensitivity analysis for evaluation of the

presented damage features. The confidence bounds generated through simulation for both features indicate positive skew in distribution, a fact compatible with the assumptions on their respective asymptotic distribution. The average Cosh distance values from 50 simulations have a much reduced, yet still largely uniform, confidence interval (from ± 50 % around the mean to ± 10 % around the mean) over different cases, while the confidence interval for average Mahalanobis distance values is expanding along x axis. The simulation mean for the Cosh distance is 8 % higher than the computed theoretical value, but their increasing tendency are almost parallel. Sensitivity analysis values for both features start quite close to the theoretical results when deviation from the original/baseline state is small, yet their difference grows larger as the deviation increases because of higher-order effects that are neglected in the linearization step of sensitivity analysis. The sensitivity analysis in this case study underestimates the feature value for significant changes in structural state/signal noise level. Note here the distribution variance terms ($trace\left[\mathbf{\Sigma}_b^{-1}\frac{d\mathbf{\Sigma}_u}{d\theta}\right]$ and $trace\left[\mathbf{\Sigma}_b^{-1}\frac{d^2\mathbf{\Sigma}_u}{d\theta^2}\right]$,) are not considered as the computation is complex and their relative influence is small.

8.4 Conclusion

This chapter proposes a sensitivity analysis approach to investigate the effect of measurement noise on two existing damage features, Mahalanobis distance of AR coefficients and Cosh distance of AR model spectra. It is found that both features values increase parabolically with respect to increases in measurement noise level. The approach is used to predict the feature values from a numerical 10-DOF bridge model in several noise level cases, and the outcome is in good agreement with that from simulated acceleration signals and theoretical calculations. This observation supports the validity of the proposed approach, which is a more efficient way to examine the behavior of damage features than repeating the simulation process for a number of times.

It is noted here that the Mahalanobis distance and Cosh distance features respond to increase in the noise level after it passes 14 % in the case study. This fact implies that both features are not completely robust to variations unrelated to structure change. This is partially due to the fact that the damage identification algorithms use only the response from a single channel, which is generated as a result of interaction between several components (structure, environment, and excitation). Thus, these damage indices are best used to monitor a structure with reasonably stable operating conditions.

Acknowledgement The research described in this chapter is supported by the National Science Foundation through Grant No. CMMI-0926898 by Sensors and Sensing Systems Program and by a grant from the Commonwealth of Pennsylvania, Department of Community and Economic Development, through the Pennsylvania Infrastructure Technology Alliance (PITA).

References

1. Doebling SW, Farrar CR, Prime MB (1998) A summary review of vibration-based damage identification methods. Shock Vib Dig 30(2):91–105
2. Ciang CC, Lee JR, Bang HJ (2008) Structural health monitoring for a wind turbine system: a review of damage detection methods. Meas Sci Technol 19(12):122001
3. Peeters B, Maeck J, De Roeck G (2001) Vibration-based damage detection in civil engineering: excitation sources and temperature effects. Smart Mater Struct 10(3):518
4. Lynch JP, Sundararajan A, Law KH, Kiremidjian AS, Carryer E (2004) Embedding damage detection algorithms in a wireless sensing unit for operational power efficiency. Smart Mater Struct 13(4):800
5. Maia NMM, Silva JMM, Almas EAM, Sampaio RPC (2003) Damage detection in structures: from mode shape to frequency response function methods. Mech Syst Signal Process 17(3):489–498
6. Hearn G, Testa RB (1991) Modal analysis for damage detection in structures. J Struct Eng 117(10):3042–3063
7. Salawu OS (1997) Detection of structural damage through changes in frequency: a review. Eng Struct 19(9):718–723
8. Worden K, Manson G, Fieller NRJ (2000) Damage detection using outlier analysis. J Sound Vib 229(3):647–667
9. Okafor AC, Dutta A (2000) Structural damage detection in beams by wavelet transforms. Smart Mater Struct 9(6):906
10. Fang X, Luo H, Tang J (2005) Structural damage detection using neural network with learning rate improvement. Comput Struct 83(25):2150–2161
11. Brockwell PJ, Davis R (2009) Time series: theory and methods. Springer, New York
12. Sohn H, Farrar CR (2001) Damage diagnosis using time series analysis of vibration signals. Smart Mater Struct 10(3):446
13. Zhang QW (2007) Statistical damage identification for bridges using ambient vibration data. Comput Struct 85(7):476–485
14. Yao R, Pakzad SN (2012) Autoregressive statistical pattern recognition algorithms for damage detection in civil structures. Mech Syst Signal Process 31:355–368
15. Nair KK, Kiremidjian AS, Law KH (2006) Time series-based damage detection and localization algorithm with application to the ASCE benchmark structure. J Sound Vib 291(1):349–368

16. Dorvash S, Pakzad SN (2012) Effects of measurement noise on modal parameter identification. Smart Mater Struct 21(6):065008
17. Mahalanobis PC (1936) On the generalized distance in statistics. Proc Natl Inst Sci Ind 2(1):49–55
18. Gray A Jr, Markel J (1976) Distance measures for speech processing. IEEE Trans Acoust Speech Signal Process 24(5):380–391
19. Brockwell PJ, Richard AD (2002) Introduction to time series and forecasting. Springer, New York
20. Chopra AK (2006) Dynamics of structures : theory & applications to earthquake engineering. Prentice Hall, Upper Saddle River, NJ
21. Porat B (1994) Digital processing of random signals: theory and methods. Prentice-Hall, Englewood Cliffs, NJ
22. James GH III, Carne TG, Lauffer JP (1993) The natural excitation technique (NExT) for modal parameter extraction from operating wind turbines. No. SAND—92-1666. Sandia National Labs., Albuquerque, NM
23. Berk KN (1974) Consistent autoregressive spectral estimates. Ann Stat 2(3):489–502